Microstructure and mechanical characterization of high strength low alloy steel welded joint by hybrid laser arc welding

Liang Liang Bao, Yong Wang and Tao Han

1 School of Materials Science and Engineering, China University of Petroleum, Tsing Dao, China
E-mail: baoliangfighting@163.com

Abstract. Hybrid laser arc welding was developed to joint EQ70 steels. Welds with no visible defects were obtained. Investigations on microstructure and mechanical properties showed that: the welded metal (WM) consisted of acicular ferrite (AF), granular bainite (GB) and M-A constituents. The arc zone and laser zone possessed semblable HAZ microstructures. Coarse grained heat affected zone (CGHAZ) and fine grained HAZ (FGHAZ) were both composed of lath martensite (LM), GB and polygonal ferrite (PF). The intercritically HAZ (ICHAZ) consisted of martensite and M-A constituents. The microstructure of the subcritically HAZ (SCHAZ) was tempered sorbite. Partly cracked blocky M-A constituents were found at the grain boundary of intercritically reheated CGHAZ (ICCGHAZ). Some M-A constituents was slender and distributed in the grain of ICCGHAZ. The arc zone and laser zone had similar hardness and micro-shear strength distributions. The highest hardness and micro-shear strength of the backing and double-pass welded joints appeared near CGHAZs, reheated WM and ICCGHAZ. Slightly soften showed up at the SCHAZs. SCHAZ, CGHAZ and ICCGHAZ showed a reduction of micro-shear toughness. -40℃ sub-size Charpy impact testing showed that FL specimens possessed the lowest impact values. The coarse CGHAZs and cracked blocky M-A constituents of ICCGHAZ may be the reason caused the toughness deterioration.

1. Introduction

Thick section high strength low alloy (HSLA) steels are widely used in ocean engineering due to good combination of strength and toughness [1]. Arc welding processes have a broad use in shipbuilding industry because of the high-quality stable process and cheap equipment. However the efficiency of arc welding processes are extremely low for the welding of thick steels owing to the low penetration depth. Multi-pass welding procedure is usually applied which inevitably increases residual stress and distortion. High energy beam welding processes such as laser welding, electron beam welding have great welding depth and efficiency. But the costs of high power special apparatuses are especially large. There is an urgent need to develop an efficient welding process suitable for the welding of thick section steels. Hybrid laser arc welding (HLAW) is a promising process which can compensate the disadvantages of laser welding and arc welding by utilizing both features [2]. With the synergistic interaction of laser and arc, HLAW allows increased gap tolerances compared with laser welding, deepen penetration and faster welding speed than arc welding [3]. HLAW is receiving extensive and continuous attention as an efficient welding technique suitable for thick section steels.

X. Cao et al. [4] developed a single-pass HLAW process to weld 9.3 mm thick HSLA-65 steel. Compared with the MIG welds, the HLAW process resulted in a less distortion welds. Ivan Bunaziv et al. [5] realized a stable double-side butt weld process of 45 mm thick high strength steel HLAW. M.

Wahha et al. [6] reported a one-pass weld of 25 mm thick plates in I-butt configuration using HLAW. The HLAW was successfully applied to double-side welding of 50 mm thick joints. No detailed information was presented about the mechanical properties of HLAW joints. Most researchers' attentions were focused on how to realize the HLAW process on thick section steels [7], the studies on microstructure and mechanical properties of the HLAW welded joints were relatively less. Yanbin Chen et al. [8] studied the microstructure and properties of a four-pass double-side HLAW welded joint and found that welded joint possessed higher strength and lower toughness than the base metal. S. Gook et al. [9] investigated the possibilities of HLAW on longitudinal welds of high strength X80 pipe steels. 23.4 mm thick section X80 steel was jointed by HLAW. The hardness and impact toughness of HLAW WM met the requirements. The microstructure and properties of HAZ were not considered in these studies. Most of the researchers are primarily concentrated on the WM of HLAW joints [10, 11], studies on HAZs were relatively few. A. E. Nolting et al. [12] joined 9.1 mm thick HSLA-65 steel plates by HLAW. The sub-size Charpy impact test found that specimens notched in the HAZ were less tough than the base metal and the HAZ impact values fluctuated greatly. In this investigation, HSLA EQ70 steel plates were welded by HLAW. The microstructure and mechanical property of the WM and HAZ were evaluated in detail.

2. Experimental procedure

2.1. Hybrid laser arc welding experiments

EQ70 steel plates and ER100S-G filler wire were used. The chemical compositions are listed in Table 1. Shielding gas of 80% Ar, 18% CO_2 and 2% O_2 with a flow rate of 20 L/min was used. Butt joint of 45° V-groove configuration with a 6 mm root face was prepared. An IPG photonics corporation (YLS-10000) fiber laser system and a Fronius (TPS-4000) welding source were used. Laser leading arc mode was selected because incomplete fusion often occurs under arc leading laser mode. The distance between laser beam and filler wire was 10 mm. The laser defocus distance was +6 mm. Laser power is the most important parameter [3]. The various laser powers in the trials were 4.5 kW, 5.5 kW and 6.5 kW. The steels were welded under different welding speed of 0.6 m/min, 0.8 m/min and 1.0 m/min.

Table 1 Chemical compositions of EQ70 and ER100S-G (wt-%).

Elements	C	Si	Mn	S	P	Cu
EQ70	0.12	0.25	1.09	0	0.004	0.28
ER100S-G	0.08	0.47	1.62	0.004	0.015	0.11
Elements	Cr	Mo	V	N	B	Al
EQ70	0.58	0.53	0.04	0.0039	0.0009	0.074
ER100S-G	0.22	0.25	/	/	/	/

2.2. Metallographic and mechanical characterization

Metallurgical specimens were etched with 4% nital solution. Lepera etchant was used to reveal M-A constituents. The microstructures were characterized by optical microscope (OM), scanning electron microscope (SEM), electron backscattered diffraction (EBSD) and transmission electron microscope (TEM). Sub-size Charpy V-notch impact specimens (55 mm×10 mm×5 mm) were tested at -40 ℃. The Vickers hardness of the arc zone (Line 1 in figure 2), laser zone (Line 2 in figure 2) and overlapping zone (Line 3 in figure 3) were measured with a force of 10 kgf (HV10) and 10 s dwell time. Micro-shear test was conducted to illustrate the variation tendency of mechanical properties. Specimens with dimensions of 2 mm×2 mm×12 mm were cut and grinded into 1.5 mm×1.5 mm×12 mm from the welded joints as shown in figure 2 and figure 3. The test was conducted at room temperature with a loading speed of 0.5 mm/min. The curves of shear load P versus the displacement of shear cutter S were recorded. The micro-shear strength τ_b and micro-shear toughness W_s are estimated referring to X. P. Zhang [13].

3. Results and Discussions

3.1. Weld formation

Figure 1 shows the weld formations under different laser power and welding speed. Lack of penetration was observed under 4.5 kW laser power. Severe collapse of molten pool occurred, when laser power reached 6.5 kW. Complete fusion was achieved under 5.5 kW laser power. 1.5 kW laser power was used in the subsequent welding passes, because high laser power may cause the turbulence of the molten pool. Joints with sufficient penetration and no visible defects were achieved under 0.6 and 0.8 m/min welding speed. Lack of penetration appeared when the welding speed was 1.0 m/min. Relative lower 0.6 m/min welding speed was selected for the backing welding pass to maintain sufficient penetration. The welding speed of subsequent welding passes was 0.8 m/min to reduce the heat input and improve welding efficiency. To match the laser powers and the welding speeds, the arc currents varied from 260 A to 280 A. The optimized welding parameters were determined in Table 2.

The backing welded joint was typical "wine-cup" shape with upper arc zone and lower laser zone as shown in figure 2. The arc zone had a wider WM than the laser zone, however the arc zone HAZ was narrower than laser zone HAZ. A high laser power of 5.5 kW and a slow welding speed of 0.6 m/min result in a higher heat input and a wider laser zone HAZ. To study the influence of subsequent bead on the backing bead, a double-pass HLAW welded joint with 15 mm penetration depth was achieved, as shown in figure 3.

Table 2 Optimized welding parameters.

Welding Pass	Laser power [kW]	Arc current [A]	Arc voltage [V]	Welding velocity [m/min]
Backing	5.5	260	26.0~26.4	0.6
Subsequent	1.5	280	25.0~26.2	0.8

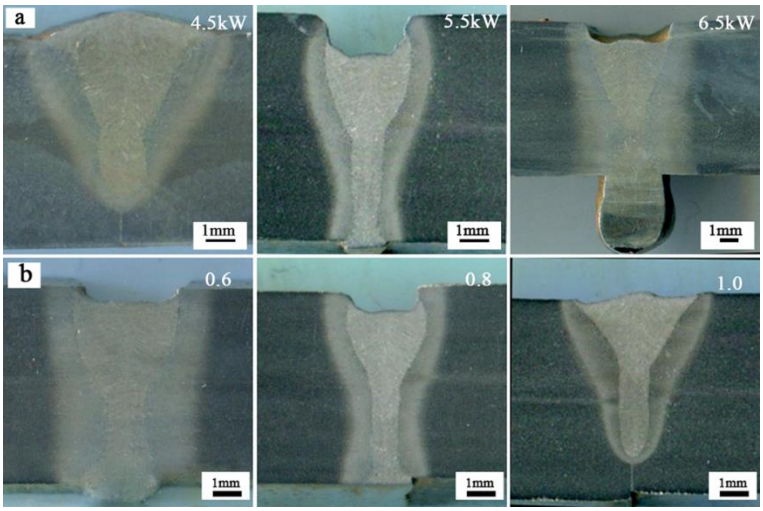

Figure 1. Weld bead profiles under different: (a) laser power, (b) welding speed.

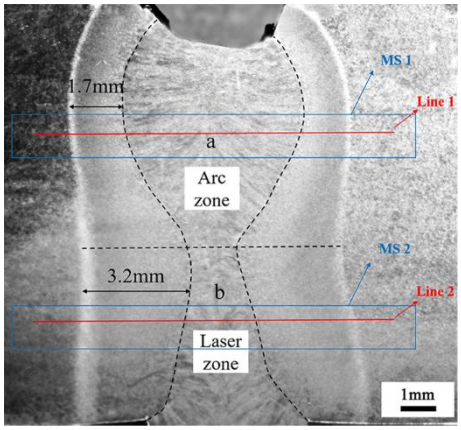

Figure 2. Weld bead profile of the backing welded joint.

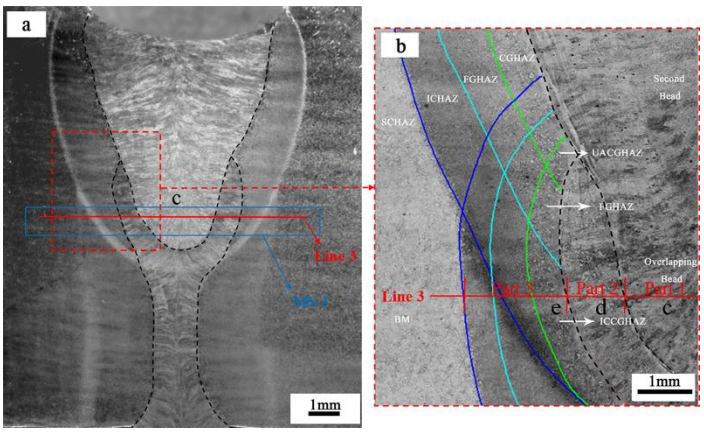

Figure 3. Weld bead profile of the double-pass welded joint.

3.2. Microstructures

Figure 4 shows the microstructures of the WM. The WM of the arc zone and laser zone were mainly composed of AF. Some GB and M-A constituents were also found in the WM. M-A constituents (reveals white and bright) were mainly scattered within the grain. The grain size of the laser zone WM was much smaller than that of the arc zone WM, relative fast cooling rate led to the small grains. The double-pass welded joint became further complicated due to the thermal cycles overlapping effect. Part of the arc zone WM went through a remelting process (point c in figure 3a). The remelt region was composed of AF, GB and a bit of LM as shown in figure 4e. Part of the arc zone WM experienced a reheating process (point d in figure 3b). Compared with the remelting WM, more GB and LM were formed in the reheat weld as shown in figure 4f.

The arc zone and laser zone possessed semblable HAZ microstructures. Figure 5 shows the arc zone HAZ microstructures. The CGHAZ and FGHAZ were both mainly composed of LM, some GB and polygonal ferrite (PF) also can be found. The ICHAZ consisted of martensite and M-A constituents, but the lath structure of martensite disappeared. The microstructure of the SCHAZ was tempered sorbite and the lath structure was visible. Reheated by the second thermal cycle, the CGHAZ was divided into unaltered CGHAZ (UACGHAZ), FGHAZ, ICCGHAZ and subcritically reheated CGHAZ (SCCGHAZ) as shown in figure 3b. The toughness deterioration always occur at the ICCGHAZ [13]. Detailed microstructure characterization of ICCGHAZ were conducted by OM, SEM as shown in figure 6. Most of the M-A constituents was blocky and distributed on the grain boundary, some M-A constituents was slender and distributed in the grain. The blocky M-A constituents was 1~2 μm. The ICCGHAZ inherited the coarse grain size of the CGHAZ. The blocky M-A constituents continuously connected with each other at the boundaries. And some of the blocky M-A constituents cracked already as shown in figure 7c and 7d.

3.3. Hardness and micro-shear properties

Figure 7 shows the Vickers hardness and micro-shear testing results. The variation tendency of the micro-shear strength was well matched with the hardness. The arc zone and laser zone of the backing welded joint had similar hardness and micro-shear strength distributions. The highest hardness and micro-shear strength of the arc zone and laser zone both appeared near the CGHAZs. Slightly soften showed up at the SCHAZs with relative lower hardness and micro-shear strength compared with base metal, because tempered sorbite was formed in SCHAZs. The hardness and micro-shear strength of the laser zone were higher than that of the arc zone, especially for the WM. The grains in the laser zone was much smaller than that of the arc zone. The small grain mains more grain boundaries per unit volume. It is generally recognized that grain boundaries can inhibit the dislocation movement and increase the hardness and strength. As for the double-pass welded joint, the reheated WM (Part 2 in

figure 3) and ICCGHAZ owned the highest hardness and micro-shear strength with values of 432 HV10 and 1100 MPa which were basically equal to that of the arc zone CGHAZ. The LM and M-A constituents in the ICCGHAZ and reheated WM led to the hardness increase. The remelt WM (Part 1 in figure 3) of the double-pass joint has a hardness of 302 HV10 and micro-shear strength of 700 MPa which were much lower than that of the backing welded joint WM. The reduction of the harden LM caused the decrease. The lowest micro-shear toughness of the arc zone and laser zone both presented at SCHAZs with values of 0.70 J/mm^2 and 0.82 J/mm^2, respectively. The low micro-shear strength of SCHAZ accounted for the low toughness. Reduction of micro-shear toughness also appeared at the arc zone and laser zone CGHAZs with average values of 0.94 J/mm^2 and 0.98 J/mm^2 despite of high micro-shear strength. The lowest micro-shear toughness of the overlapping zone presented at SCHAZ (0.74 J/mm^2) and ICCGHAZ (0.72 J/mm^2). Obviously, the subsequent thermal cycle deteriorated the CGHAZ micro-shear toughness. The SCHAZ, CGHAZ and ICCGHAZ were the local brittle zones.

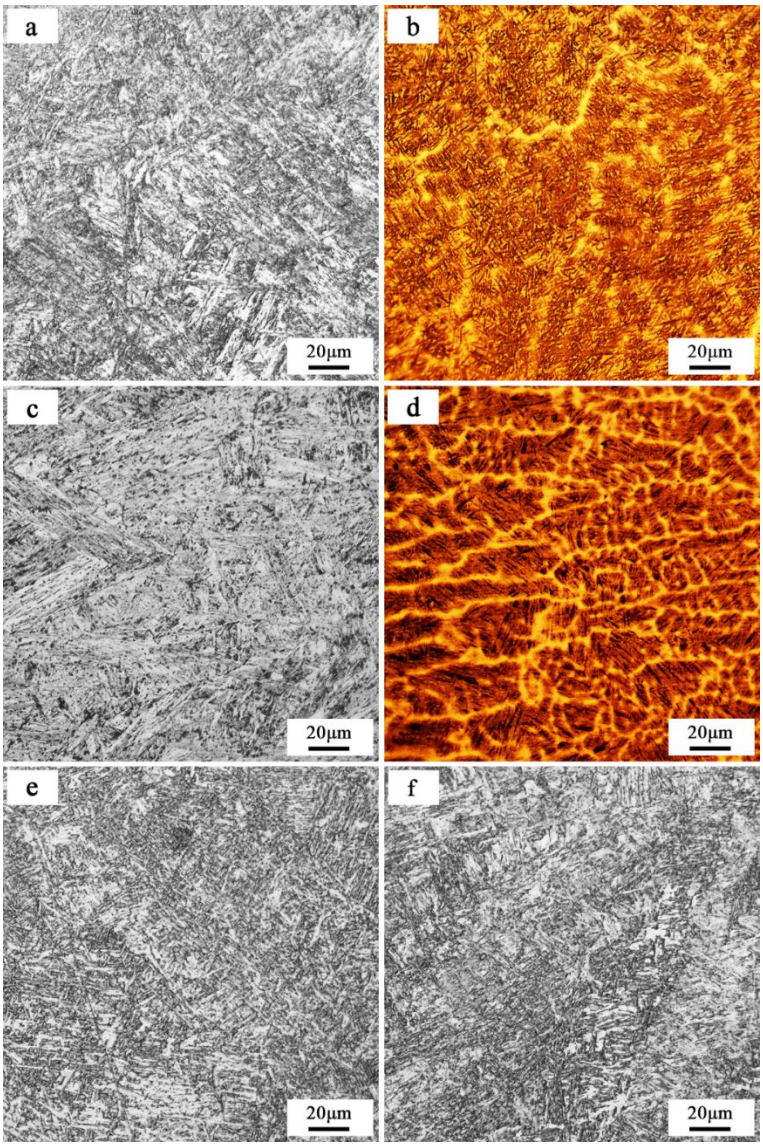

Figure 4. Optical microstructures of WM: (a), (b) are arc zone at point a in figure 2, (c), (d) laser zone at point b in figure 2, (e) overlapping zone at point c in Figure 3b, (f) overlapping zone at point d in figure 3b (a, c, e, f were etched with 4% nital solution and b, d were etched with Lepera etchant).

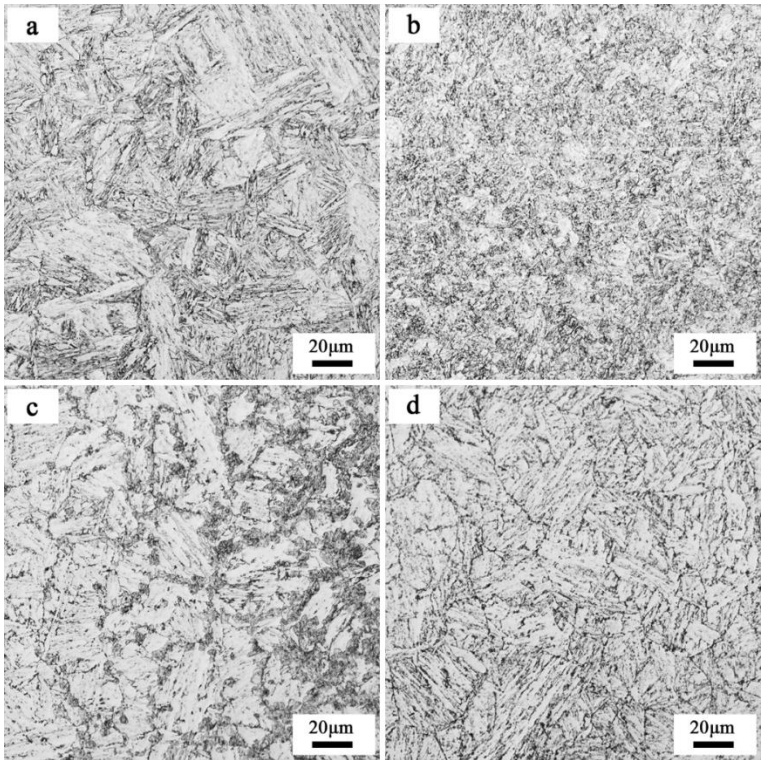

Figure 5. Microstructures of the arc zone: (a) CGHAZ, (b) FGHAZ, (c) ICHAZ, (d) SCHAZ.

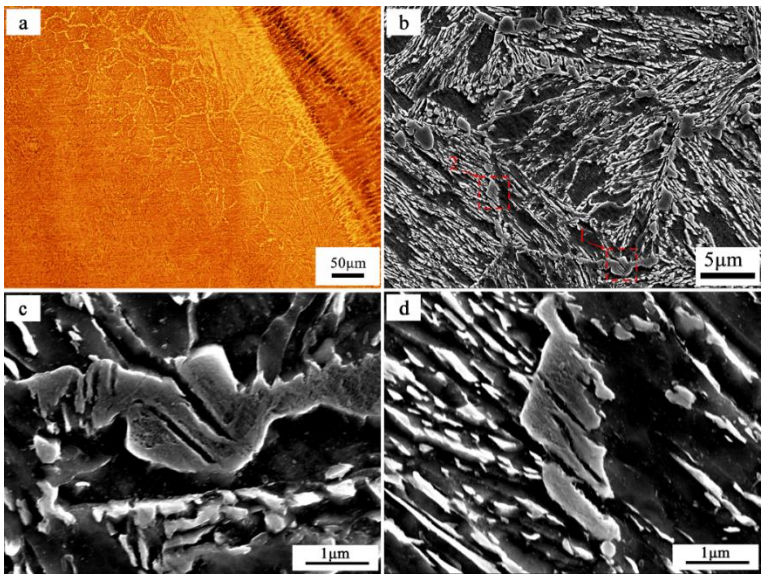

Figure 6. Microstructure characterization of ICCGHAZ: (a) OM micrograph by Lepera etchant (b) SEM micrograph, (c) enlarged SEM micrograph of region 1, (d) enlarged SEM micrograph of region 2.

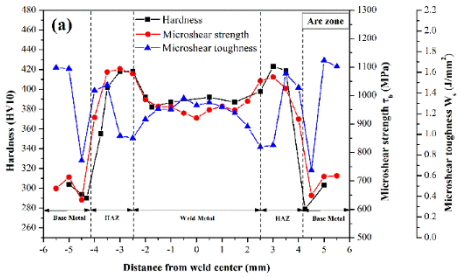

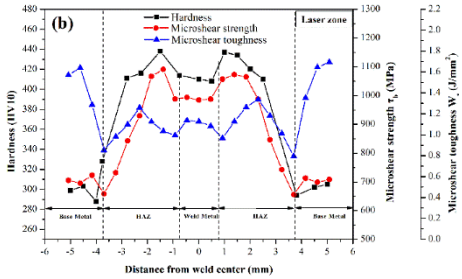

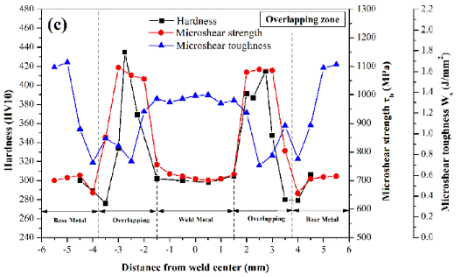

Figure 7. Vickers hardness and micro-shear properties of: (a) arc zone (MS 1), (b) laser zone (MS 2), (c) overlapping zone (MS 3).

3.4. -40 ℃ Charpy impact toughness

The sampling location are shown in figure 8. The V-notch was placed at the welded metal center (WM), fusion line (FL) and fusion line +2 mm (FL+2). The results were shown in figure 9. The average impact values of base metal was 61.3 J. The FL specimens possessed of the lowest impact values. The average impact values of the arc zone and laser zone FL specimens were 35.7 J and 32 J, respectively. The overlapping zone FL specimen owned an average impact value of 27.3 J. To identify the microstructures that caused toughness deterioration, the macro-fracture and micro-fracture morphologies of the base metal and FL specimens were characterized by stereomicroscope and SEM.

As shown in figure 10, the macro-fracture surface of the base metal was dark and uneven, the shear lip nearly accounted for half of the fracture surface. The micro-fracture surface was a typical dimple ductile fracture with large dimples linked by small dimples as shown in figure 11a. As for the arc zone and laser zone FL specimens, the notches crossed the WM and CGHAZs. Despite of the large percentage of shear lip similar to the base metal specimen, the fibrous zone was very small and most of the macro-fracture surface was radiative zone characterized by bright and even surface. Figure 12b and figure 12d are the micro-fracture morphologies of point b (in Figure 10b, arc zone CGHAZ) and point d (in figure 10.c, laser zone CGHAZ). The surface was quasi-cleavage fracture featured with fracture facet and tear ridges. The fracture facets varied from several to dozens of microns, some dimples were distributed around the tear ridges. Figure 11c and figure 11e are the micro-fracture morphologies of point c (in figure 10b, arc zone WM) and point e (in figure 10c, laser zone WM). The morphologies were both typical dimple fracture surface. The dimples at point c were uniform sized but smaller than that of the point e. With overall consideration of macro-fracture and micro-fracture morphologies, it can be inferred that the CGHAZs caused the toughness deterioration of the arc zone FL and laser zone FL specimens. The coarse CGHAZs may be the reason caused the toughness deterioration. As for the overlapping FL specimen, the shear lip was the smallest only 20% of the fracture surface and its macro-fracture surface was bright white and flat. There was basically no fibrous zone. Figure 11f and figure 11g are the micro-fracture morphologies of point f (in figure. 10d, ICCGHAZ) and point g (in figure. 10d, reheated WM). The micro-fracture morphology at reheated WM was typical dimple. The micro-fracture morphology at ICCGHAZ was quasi-cleavage fracture and the fracture facets were larger than that of the CGHAZs (figure 11d and figure 11d). The ICCGHAZ led to the toughness reduction of the overlapping FL specimen.

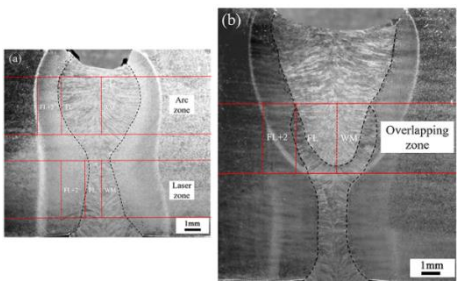

Figure 8. Impact sampling location for: (a) single-pass welded joint, (b) double-pass welded joint.

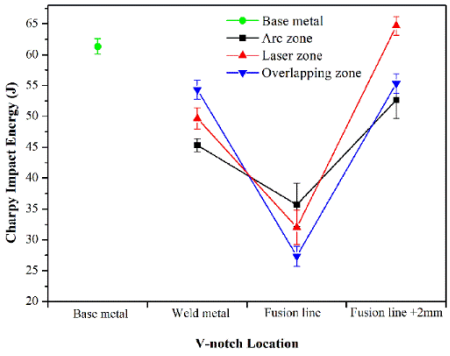

Figure 9. Charpy impact testing results.

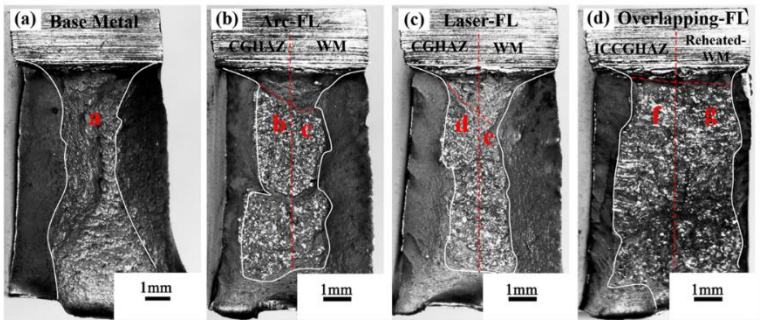

Figure 10. Macro-fracture morphologies of: (a) base metal, (b) arc zone FL, (c) laser zone FL and (d) overlapping zone FL.

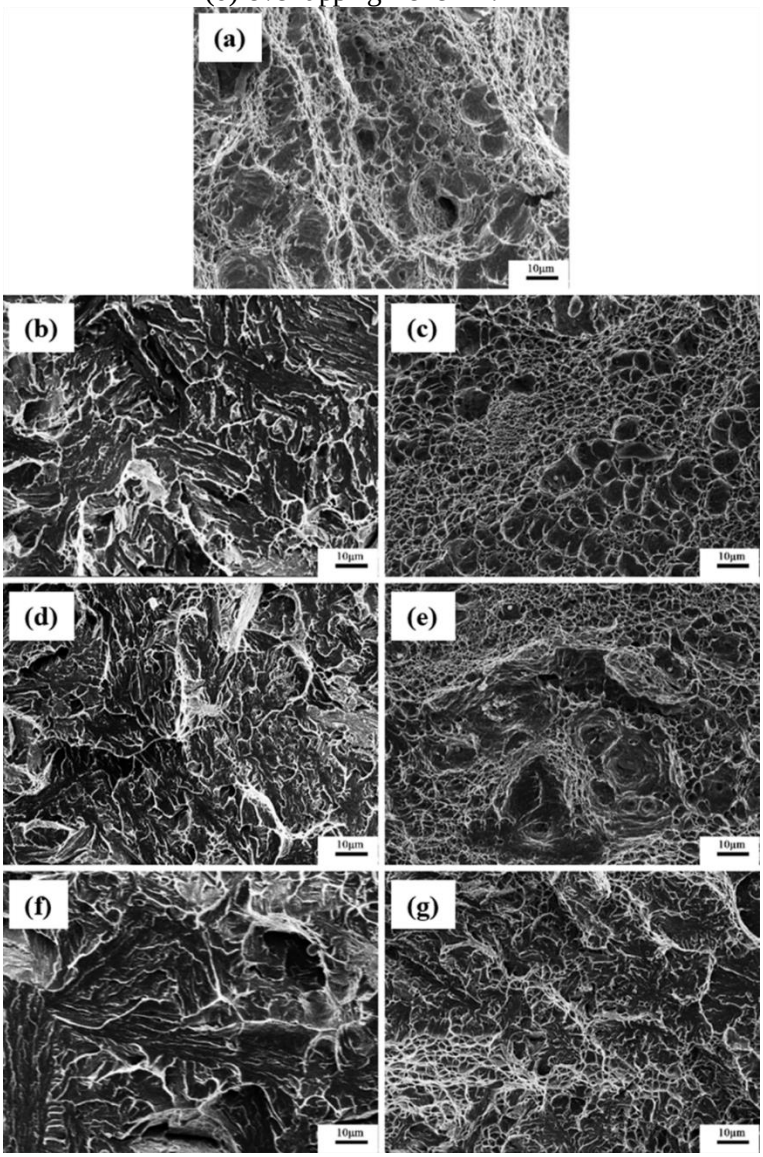

Figure 11. Micro-fracture morphologies of: (a) point a in figure 10a, (b) point b in figure 10b, (c) point c in figure 10b (d) point d in figure. 10c, (e) point e in figure 10c, (f) point f in figure 10d, (g) point g in figure 10d.

4. Conclusion

The backing and double-pass HLAW welded joints with no visible defects were obtained under optimised parameters. Arc zone WM, laser WM and overlapping zone WM both consisted of AF, GB and M-A constituents. Arc zone and laser zone HAZs had similar microstructures. CGHAZs were composed of LM, GB and PF. ICCGHAZ inherited the coarse grain size of CGHAZ and cracked blocky M-A constituents were found at grain boundary. The variation tendency of the micro-shear strength was well matched with the hardness. The highest hardness and micro-shear strength appeared near CGHAZs, reheated WM and ICCGHAZ. Slightly soften showed up at SCHAZs. SCHAZ, CGHAZ and ICCGHAZ showed a reduction of micro-shear toughness. -40℃ sub-size Charpy impact testing showed that FL specimens possessed the lowest impact values. The coarse CGHAZs and cracked blocky M-A constituents of ICCGHAZ may be the reason caused the toughness deterioration.

5. References

[1] Blekkenhorst F, Ferrari GM, Wekken CJVD, et al. 1986 *Br Corros J* **21(3)**: 163-176
[2] Flemming Ove Olsen 2009 *Hybrid Laser-Arc Welding* (UK: Woodhead Publishing Limited)
[3] Acherjee B. 2018 Opt Laser Technol **99** 60-71
[4] Cao X, Wanjara P, Huang J, et al. 2011 *Mater Des* **32(6)** 3399-3413
[5] Bunaziv I, Frostevarg J, Akselsen O M, et al. 2018 *J Mater Process Technol* **102** 34-44
[6] Wahba M, Mizutani M, Katayama S 2016 *Mater Des* **97** 1-6
[7] Gu X, Li H, Jiang X, et al. 2017 *Int J Adv Manuf Technol* **89(9-12)** 1-11
[8] Chen Y, Feng J, Li L, et al. 2013 *Mater Sci Eng A* **582** 284-293
[9] Gook S, Gumenyuk A, Rethmeier M. 2014 *Sci Technol Weld Joi* **19(1)** 15-24
[10] Chen Y, Yang C, Chen H, et al. 2015 *Int J Adv Manuf Techno* **78(1-4)** 457-464
[11] Zhang X, Mi G, Li S, et al 2017 *Int J Adv Manuf Techno* **3** 1-12
[12] Nolting AE, Munro C, Cao XJ, et al.2012 *Can Metall Quart* **51(3)** 336-345.
[13] P. Zhang X, Dorn L 1998 *Int J Pres Ves Pip* **75** 37-42

Acknowledgments

This work was supported by the National Natural Science Foundation of China (No.51874345), Natural Science Foundation of Shandong Province (No.ZR2018MEE012) and Key Research & Development project of Shandong Province (No.2017CXGC0812).